solvent removal under high vacuum gave a crude product that was chromatographed on silica gel (elution with pentane) to provide hydrocarbon **22d** (6.4 mg, 62%): mp 116-117 °C; ^{1}H NMR ($CDCl_3$, 300 MHz) δ 1.11-1.32 (m, 11 H), 1.54-1.91 (m, 15 H); ^{13}C NMR ($CDCl_3$, 22.5 MHz) δ 47.68, 47.51, 41.22, 32.94, 30.18, 25.19; mass spectrum, m/z 242 (91%, M^+).

Monoolefin 30. Triene **3** (25 mg, 0.10 mmol) was dissolved in 10 mL of hexane, and 5% Rh on carbon (20 mg) was added. After degassing, the solution was shaken under an atmosphere of hydrogen gas (48 psi) for 60 h at room temperature. Filtration and removal of solvent yielded monoolefin **30** as the sole product (19.6 mg, 81%): mp 162-163 °C; ^{1}H NMR ($CDCl_3$, 300 MHz) δ 1.3-2.2 (m, 24 H), 2.3-2.56 (m, 4 H); ^{13}C NMR ($CDCl_3$, 22.5 MHz) δ 129.02, 32.37, 31.06, 26.05, 25.75, 24.38; mass spectrum, m/z 244 (100%, M^+).

Acknowledgment. This work was supported by grants from the donors of the Petroleum Research Fund, administered by the American Chemical Society, the National Science Foundation (Grant CHE-8207890 to J.M.), and the National Institutes of Health (Grant CA-24487 to J.C.). The photoelectron spectroscopy was funded by grants from the Deutsche Forschungsgemeinschaft, the Fonds der Chemischen Industrie, and the BASF Aktiengesellschaft (to R.G.). We thank A. Flatow for recording the PE spectra.

Registry No. 3, 91266-48-7; **6**, 91266-53-4; (*cis*)-**6** (thiirane), 101713-72-8; (*trans*)-**6** (thiirane), 101713-73-9; **9**, 80427-20-9; **10**, 91266-49-8; (*E*)-**11**, 101713-64-8; (*Z*)-**11**, 101713-65-9; (*cis*)-**12**, 101713-68-2; (*trans*)-**12**, 101713-69-3; (*cis*)-**12** (hydrazine), 101713-66-0; (*trans*)-**12** (hydrazine), 101713-67-1; (*cis*)-**12** (deprotected), 101713-70-6; (*trans*)-**12** (deprotected), 101713-71-7; **13**, 91266-54-5; **14**, 6051-37-2; **22a**, 101713-74-0; **22b**, 101713-75-1; **22c**, 101713-76-2; **22d**, 101713-77-3; **22e**, 101713-78-4; **26**, 101713-79-5; **27**, 101713-80-8; **28**, 101713-81-9; **29**, 101713-82-0; **29** (trifluoroacetate), 101759-50-6; **30**, 101713-83-1; $H_2NNHPO(OEt)_2$, 56183-69-8; 1,4-cyclohexanedione, 637-88-7.

Solid-State ^{2}H NMR, ^{57}Fe Mössbauer, and X-ray Structural Characteristics of μ_3-Oxo-Bridged Mixed-Valence $[Fe_3O(O_2CCH_3)_6(4\text{-Me-py})_3](C_6H_6)$: Dynamics of the Benzene Solvate Molecules Influencing Intramolecular Electron Transfer

Scott E. Woehler,[1] R. J. Wittebort,*[1] Seung M. Oh,[2] David N. Hendrickson,*[2] Daryl Inniss,[3] and Charles E. Strouse*[3]

Contribution from the Department of Chemistry, University of Louisville, Louisville, Kentucky 40292, the School of Chemical Sciences, University of Illinois, Urbana, Illinois 61801, and the Department of Chemistry and Biochemistry, University of California, Los Angeles, California 90024. *Received October 28, 1985*

Abstract: Intramolecular electron transfer is investigated in the mixed-valence complex $[Fe_3O(O_2CCH_3)_6(4\text{-Me-py})_3](C_6H_6)$, where 4-Me-py is 4-methylpyridine. Rotational motion of the benzene solvate molecule and the possible influence of this motion on the rate of intramolecular electron transfer are studied crystallographically and spectroscopically. The compound crystallizes in the rhombohedral space group $R32$; $a = b = 18.552$ (3) Å, $c = 10.556$ (2) Å at 133 K with $Z = 3$. The final discrepancy factors are $R = 0.048$ and $R_w = 0.061$ for 1209 reflections with $I > 3\sigma(I)$. Complex molecules and disordered benzene solvate molecules are stacked in alternate sites of 32 symmetry along the 3-fold c axis. The unit cell contains three such stacks related by a 3_1 axis. The 4-Me-py ligands are nearly coplanar with the Fe_3O moiety. The 3_1 axis passes through the three nearly parallel 4-Me-py ligands of three adjacent stacks. The interligand separation, $c/3 = 3.51$ Å, along the 3_1 axes probably controls the size of the solvate cavity along the 3-fold axis. Electron density maps indicate a preferred orientation for the benzene solvate molecule with its 6-fold axis perpendicular to both the crystallographic 3-fold and 2-fold axes. The large thermal parameter observed for the solvate molecule is consistent with a dynamic disorder of this group. Two doublets of area ratio 2:1 (Fe^{III}:Fe^{II}) are present in the Mössbauer spectrum at temperatures approaching liquid helium. As the sample temperature is increased above ~60 K, the spectrum changes to eventually become a single average-valence doublet at temperatures above ~200 K. The complex $[Fe_3O(O_2CCH_3)_6(4\text{-Me-py})_3](C_6D_6)$, in which perdeuteriobenzene is the solvate molecule, gives high-resolution ^{2}H NMR spectra. Spectra are readily obtained from three sample types: random powders, magnetically oriented microcrystals, and single crystals. The spectral properties are determined both by the motionally averaged ^{2}H quadrupolar coupling and by dipolar interactions of the deuterons with the unpaired electrons of the neighboring trinuclear complexes. These two types of interactions are readily separated in the ^{2}H NMR experiment. Single-crystal ^{2}H NMR data were obtained at room temperature by rotating a ~1 × 1 × 1 mm crystal about three mutually orthogonal axes. Temperature studies were also carried out for powdered and magnetically oriented microcrystalline samples in the range of ~150-293 K. From the orientation and magnitude of the residual ^{2}H quadrupolar coupling, it was concluded that the benzene solvate molecules are not only ring rotating about their C_6 axes, but they are also rotating about the C_3 stacking axes. An appreciable through-space dipolar interaction of the magnetic dipole of the deuterons with the magnetic dipoles of the nearby paramagnetic Fe_3O complexes is present.

The general goal in the study of mixed-valence transition-metal complexes has been to understand what factors determine the rate of electron transfer between well-separated metal ions through variation of the bridge between the metal centers.[4] It is frequently implicitly assumed[5] for a symmetric binuclear mixed-valence complex that the electronic coupling between the two metal ions

(1) University of Louisville.
(2) University of Illinois.
(3) University of California.

(4) For recent reviews see: (a) Day, P. *Intl. Rev. Phys. Chem.* **1981**, *1*, 149. (b) *Mixed-Valence Compounds, Theory and Applications in Chemistry, Physics, Geology and Biology*; Brown, D. B., Ed.; Reidel: Boston, 1980. (c) Creutz, C. *Prog. Inorg. Chem.* **1983**, *30*, 1-73. (d) Richardson, D. E.; Taube, H. *Coord. Chem. Rev.* **1984**, *60*, 107-129.

0002-7863/86/1508-2938$01.50/0

and the magnitude of vibronic coupling between the d electrons and the molecular distortion are the two most important factors. In most studies, the environment about a mixed-valence complex in the solid state has not been implicated as an important factor controlling the rate of electron transfer.

The results of very recent experiments show that mixed-valence iron acetates of the composition $[Fe_3O(O_2CCH_3)_6(L)_3]S$ are well-suited for determining how important the solid-state environment is in controlling intramolecular electron transfer. In these complexes, L is pyridine or a substituted pyridine and S is a solvate molecule such as benzene, chloroform, or a pyridine molecule. In a recent communication,[6] we showed that a change in the solvate molecule dramatically affects the intramolecular electron-transfer rate in the solid state. It was suggested that the dynamic disorder of the ligands L and/or solvate molecules determines the rate of *intra*molecular electron transfer in the Fe_3O complexes. As the temperature of the sample is increased, the onset of motion of L and/or S leads to an appreciable increase in the rate of electron transfer.

In this paper, the first definitive evidence for dynamics of a solvate molecule will be presented for $[Fe_3O(O_2CCH_3)_6(4\text{-Me-py})_3](C_6D_6)$, where 4-Me-py is 4-methylpyridine. Well-resolved ^2H NMR spectra have been obtained for this complex. The aim of these ^2H NMR studies is to examine solvate molecule dynamics by measuring the residual quadrupolar coupling constant of the benzene deuterons. ^2H NMR spectroscopy has proven useful in studying dynamics both in diamagnetic[7] and, to a more limited degree, paramagnetic[8] complexes. The mixed-valence iron acetate complexes have $S = 1$ ground states.[9] In the present studies, dipolar interactions of the solvate deuteron magnetic dipole with the magnetic dipole of the nearby paramagnetic Fe_3O complexes are seen. These interactions could prove to be quite useful in probing the electronic structure of mixed-valence complexes. Furthermore, it will be shown that microcrystalline samples of these Fe_3O complexes strongly orient in the 5.9-T field of the ^2H NMR spectrometer. Thus, one has the option of studying randomly or magnetically oriented powders as well as single crystals. Spectra of all three sample types are reported herein and are used to determine the amplitude and rate (a lower limit) of solvate dynamics. In combination with magnetic susceptibility measurements, the paramagnetic shifts are used to probe the spatial extent of the magnetic moment of the mixed-valence Fe_3O complex. Finally, the results of a single-crystal X-ray structure at 133 K and variable-temperature ^{57}Fe Mössbauer studies of $[Fe_3O(O_2CCH_3)_6(4\text{-Me-py})_3](C_6H_6)$, **1**, are presented and analyzed to show what influence the benzene solvate molecule has on the rate of electron transfer. Preliminary results of this study have been communicated.[10]

Experimental Section

Compound Preparation. 4-Methylpyridine was dried by refluxing over BaO and fractionally distilled under an argon atmosphere. Benzene was dried with Na/benzophenone and distilled. Benzene-d_6 (99.5 atom % deuterium) was purchased from Aldrich Chemical Co. and was used without further purification. Elemental analysis was performed in the Microanalytical Laboratory of the School of Chemical Sciences, University of Illinois. Purified solvents and compounds were always stored and manipulated in an inert-atmosphere glovebox under an argon atmosphere.

Samples of $[Fe_3O(O_2CCH_3)_6(4\text{-Me-py})_3](C_6H_6)$ were prepared by first dissolving 5 g (8.4 mmol) of $Fe_3O(O_2CCH_3)_6(H_2O)_3$ in 25 mL of 4-methylpyridine at 50–60 °C. This reaction mixture was stirred for 1 h and then slowly evaporated for 3 days. The black crystalline product $[Fe_3O(O_2CCH_3)_6(4\text{-Me-py})_3](4\text{-Me-py})$ was filtered off and stored under an argon atmosphere in a glovebox. Approximately 5 g of this compound was dissolved in ~30 mL of benzene and then slowly evaporated for 2 days. The resulting shiny crystalline product was filtered off and dried under vacuum. A crystal from this preparation was used for the X-ray structural determination. Anal. Calcd for $C_{36}Fe_3H_{45}N_3O_{13}$: C, 48.30; Fe, 18.71; H, 5.07; N, 4.69. Found: C, 47.87; Fe, 18.55; H, 5.03; N, 4.65. The C_6D_6-solvated sample was prepared with the same method using C_6D_6 as the solvent.

Table I. Crystallographic Data

formula	$[Fe_3O(O_2CCH_3)_6(4\text{-Me-py})_3](C_6H_6)$
cryst dimensions, mm	0.42 × 0.36 × 0.32
space group	$R32$
Z	3
a, Å	18.552 (3)
b, Å	18.552 (3)
c, Å	10.556 (2)
vol, Å^3	3139
density (calcd, g/cm^3)	1.42
radiation, Å	Mo, 0.7107
temp, K	133
scan rate, deg/min	6
scan mode	θ–2θ
2θ max, deg	54
total reflections	1359
reflections ($I > 3\sigma(I)$)	1209
R	0.048
R_w	0.061
EOF	2.09
no. of parameters refined	78

Experimental Methods. Variable-temperature magnetic susceptibility data were obtained for $[Fe_3O(O_2CCH_3)_6(4\text{-Me-py})_3](C_6H_6)$ on a Series 800 VST-50 SQUID susceptometer (S.H.E. Corp.) maintained by the Physics Department, University of Illinois. A magnetic field of 1 T was used. A diamagnetic correction, estimated from Pascal's constants, was used in the calculation of molar paramagnetic susceptibilities. A table of data is available in the supplementary material.

Mössbauer data were collected on a previously described[11] apparatus. The sample temperatures, controlled by a Lake Shore Cryotronics Model DRC 80C temperature controller in conjunction with a silicon diode mounted on the copper sample cell holder, are estimated to have an absolute accuracy of 3 K. The Mössbauer data were computer fit to Lorentzian line shapes with the use of a previously described[12] program. The isomer shift values are reported relative to iron foil at 298 K but are not corrected for the temperature-dependent second-order Doppler shift.

^2H NMR experiments were performed on a home-built 5.9-T spectrometer described elsewhere.[13,14] The pulse sequences used were either a standard quadrupole echo, $[(90)_x$–t–$(90)_y$–t-observe], or the sequence $[(90)_x$–$t/2$–$(180)_y$–$t/2$–$(90)_y$–$t/2$–$(180)_y$–$t/2$-observe], which refocuses both the quadrupolar and paramagnetic couplings.[15] In both sequences, a value of $t = 35$ μs was used. For the latter experiment, this requires a probe–receiver recovery time of less than 18 μs.

NMR samples were ~50 mg of tightly or loosely packed microcrystalline material sealed into a Delrin tube ($^1/_4 \times {}^1/_2$ in.). In the case of the single-crystal work, a crystal ~1 mm on each edge was epoxied into a three-sided box which could then be systematically rotated about axes perpendicular to the three orthogonal box faces. For the three orthogonal rotations, the rotation axis was perpendicular to H_0.

Crystal Measurements and Data Collection. A black crystal of $[Fe_3O(O_2CCH_3)_6(4\text{-Me-py})_3](C_6H_6)$, **1**, (0.42 × 0.36 × 0.32 mm) was used for data collection at the University of California. The 133 K data set was collected on a locally modified Picker diffractometer with a gas stream low-temperature device. The crystal was mounted on a glass fiber. The unit cell parameters were obtained by a least-squares fit to the automatically centered settings for 24 reflections. Experimental parameters associated with the data collection can be found in Table I. Three reflections monitored after every 97 reflections showed no significant variation in intensity. Intensities were derived from an analysis of the scan profiles.[16] The data were corrected for Lorentz and polarization

(5) Wong, K. Y.; Schatz, P. N. *Prog. Inorg. Chem.* **1981**, *28*, 369.
(6) Oh, S. M.; Hendrickson, D. N.; Hassett, K. L.; Davis, R. E. *J. Am. Chem. Soc.* **1984**, *106*, 7984.
(7) Griffin, R. G. *Methods Enzymol.* **1981**, *72*, 108–174.
(8) Soda, G.; Chiba, T. *J. Chem. Phys.* **1969**, *50*, 439.
(9) (a) Wrobleski, J. T.; Dziobkowski, C. T.; Brown, D. B. *Inorg. Chem.* **1981**, *20*, 684. (b) **1981**, *20*, 671. (c) Tsukerblat, B. S.; Belinskii, M. I.; Kuyavskaya, B. Ya. *Inorg. Chem.* **1983**, *22*, 995.
(10) Oh, S. M.; Kambara, T.; Hendrickson, D. N.; Sorai, M.; Kaji, K.; Woehler, S. E.; Wittebort, R. J. *J. Am. Chem. Soc.* **1985**, *107*, 5540–5541.
(11) Cohn, M. J.; Timken, M. D.; Hendrickson, D. N. *J. Am. Chem. Soc.* **1984**, *106*, 6683.
(12) Chrisman, B. L.; Tumolillo, T. A. *Comput. Phys. Commun.* **1971**, *2*, 322.
(13) Wittebort, R. J.; Subramanian, R.; Kulshreshtha, N. P.; DuPre, D. B. *J. Chem. Phys.* **1985**, *83*, 2457.
(14) Woehler, S. E.; Wittebort, R. J. *J. Magn. Reson.*, in press.
(15) Siminovitch, D. J.; Rance, M.; Jeffries, K. R.; Brown, M. F. *J. Magn. Reson.* **1984**, *58*, 62.

Table II. Positional Parameters

atom	X/a	Y/b	Z/c
Fe	0.10280 (5)	0.0000	0.0000
O(1)	0.0633 (2)	-0.1011 (2)	0.1239 (3)
O(2)	-0.0738 (2)	-0.1555 (2)	0.1468 (3)
C(1)	-0.0054 (3)	-0.1521 (3)	0.1711 (5)
C(2)	-0.0089 (4)	-0.2137 (5)	0.2652 (9)
N(10)	0.2211 (3)	0.0000	0.0000
C(11)	0.2231 (3)	-0.0713 (3)	-0.0082 (5)
C(12)	0.2961 (4)	-0.0736 (4)	-0.0097 (6)
C(13)	0.3717 (4)	0.0000	0.0000
C(14)	0.4529	0.0000	0.0000
O	0.0000	0.0000	0.0000
H(2)	0.0257	-0.2354	0.2512
H(2A)	-0.0672	-0.2621	0.2639
H(2B)	0.0045	-0.1869	0.3490
H(11)	0.1625	-0.1256	-0.0109
H(12)	0.2985	-0.1259	-0.0247
H(14)	0.4843	0.0184	0.0622
H(14A)	0.4844	0.0335	-0.0751
H(14B)	0.4380	-0.0592	-0.0115
	For Group Atoms		
C(21)	0.0000	0.0000	0.6317
C(22)	0.0649	0.0000	0.5658
C(23)	-0.0649	0.0000	0.5658
C(24)	0.0000	0.0000	0.3683
C(25)	0.0649	0.0000	0.4342
C(26)	-0.0649	0.0000	0.4342
H(21)	0.0000	0.0000	0.7264
H(22)	0.1116	0.0000	0.6132
H(23)	-0.1116	0.0000	0.6132
H(24)	0.0000	0.0000	0.2736
H(25)	0.1116	0.0000	0.3868
H(26)	-0.1116	0.0000	0.3868

effects. Because of the small variation in the transmission factors (0.69 - 0.73), no absorption correction was applied.

Structure Solution and Refinement. Direct methods (MULTAN) were used to solve the structure in the space group $R32$. The unique non-hydrogen atoms were located by successive cycles of full-matrix least-squares refinement and difference Fourier synthesis. The solvate molecule was modeled as a rigid group (C–C = 1.39 Å, C–H = 1.00 Å). The molecular orientation was based on the observation of electron density maxima on the c axis and in the ac plane consistent with the benzene geometry. The only refined parameter associated with the benzene molecule was an isotropic group temperature factor. Refinements were carried out with the solvate molecule in alternate orientations, but none of these produced an improved model.

Hydrogen atoms were included as fixed contributors to the final refinement cycles. The hydrogen atoms on the pyridine ring were found in an electron density difference map, as was at least one hydrogen atom for each of the methyl groups. The other methyl hydrogen atoms were calculated[16] based on idealized geometry (sp^3) and bond lengths (C–H = 1.00 Å). The crystallographic 2-fold axes require a disorder of the methyl hydrogen atoms of the 4-Me-py group. All hydrogen atoms were assigned temperature factors greater than or equal to those of the carbon atoms to which they are attached. The refinement converged at R = 0.048 and R_w = 0.061. The largest features in the final difference map were peaks of 0.46 e/Å^3 located near the iron atom and of 0.36 e/Å^3 located near the solvate.

Theory for ^{2}H NMR Studies

The nuclear spin Hamiltonian for solid-state deuterium NMR of paramagnetic molecules has been discussed previously by Chiba and Soda.[8] Here we address, in particular, polynuclear clusters. Neglecting homonuclear deuterium couplings, which are generally too small to be resolved in experiments with selectivity deuterated molecules containing abundant ^{1}H atoms, the Hamiltonian contains three terms:

$$H = H_Z + H_Q + H_P \quad (1)$$

H_Z is the usual zero-order Zeeman coupling and H_Q and H_P are two angular-dependent first-order terms. H_Q is the quadrupolar coupling of the spin 1 deuteron, and H_P accounts for the dipolar coupling of the deuteron with the thermally averaged classical magnetic moments, $\langle\mu\rangle$, resulting from the fast relaxing electron spins.[17] The effect of these two first-order terms in solids[17] is to split, with a coupling constant ω_Q, the ^{2}H NMR spectrum into a quadrupole doublet offset from the zero-order Zeeman frequency, by an amount ω_P, dependent on the paramagnetic dipolar coupling. This scheme is shown in Figure 1. The zero-order Zeeman frequency, γH_0, is experimentally determined by measuring the ^{2}H frequency of an isotropic diamagnetic sample such as liquid D_2O. A particularly useful feature of this experiment is that the quadrupolar and paramagnetic couplings, which report on different molecular properties, are readily separated by inspection.

Consistent with the above scheme and that the offset to the Zeeman frequency is linear in the magnetic field strength, H_0, H_P can be expressed in the convenient form

$$H_P = H_0^+ \cdot P \cdot I \quad (2)$$

which is analogous to a chemical shielding interaction where the

Table III. Bond Distances and Angles for $[Fe_3O(O_2CCH_3)_6(4\text{-Me-py})_3](C_6H_6)$

	Interatomic Distance, Å		
Fe	O		1.9071 (9)
Fe	O(2)		2.043 (3)
Fe	O(1)		2.095 (3)
Fe	N(10)		2.195 (5)
O(1)	C(1)		1.250 (6)
O(1)	O(2)		2.231 (5)
O(1)	C(2)		2.363 (8)
O(2)	C(1)		1.265 (6)
O(2)	C(2)		2.340 (7)
C(1)	C(2)		1.491 (8)
N(10)	C(11)		1.344 (5)
N(10)	C(12)		2.390 (7)
C(11)	C(12)		1.376 (7)
C(11)	C(13)		2.390 (9)
C(12)	C(13)		1.388 (7)
C(13)	C(14)		1.506 (11)
	Bond Angles, deg		
O	Fe	O(1)	95.61 (9)
O(1)	Fe	N(10)	84.39 (9)
C(1)	O(1)	Fe	133.97 (32)
O(1)	C(1)	O(2)	125.08 (46)
O(1)	C(1)	C(2)	118.88 (48)
O(2)	C(1)	C(2)	116.03 (47)
C(11)	N(10)	C(11)	117.40 (64)
C(11)	N(10)	Fe	121.30 (32)
N(10)	C(11)	C(12)	122.88 (56)
C(11)	C(12)	C(13)	119.64 (57)
C(12)	C(13)	C(12)	117.53 (71)
C(12)	C(13)	C(14)	121.24 (35)

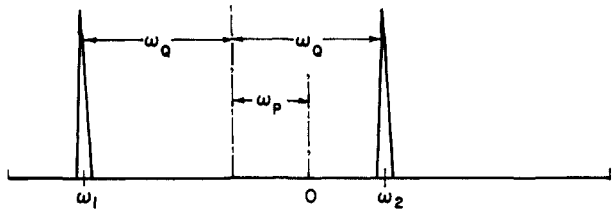

Figure 1. Spectral splitting pattern for a deuteron with quadrupolar splitting ω_Q and paramagnetic coupling ω_P. $\omega_Q = {}^1/_2(\omega_1 - \omega_2)$ and $\omega_P = {}^1/_2(\omega_1 + \omega_2)$.

(16) The programs used in this work included modified versions of the following programs: CARESS (Broach, Coppens, Becker, and Blessing), peak profile analysis and Lorentz and polarization corrections; MULTAN (Main), package of programs, including direct methods, structure factor normalization, Fourier transform, and peak search; ORFLS (Busing, Martin, and Levy), structure factor calculation and full-matrix least-squares refinement; ORFFE (Busing, Martin, and Levy), distance, angle, and error calculations; ABSORB (Coppens, Edwards, and Hamilton), absorption correction calculation; ORTEP (Johnson) figure plotting; HYDROGEN (Trueblood), calculation of hydrogen atomic positions. All calculations were performed on a DEC VAX 11/750 computer.

(17) Shulman, R. G.; Jaccarino, V. *Phys. Rev.* **1957**, *108*, 1219.

coupling tensor, P, takes the place of the usual diamagnetic chemical shielding tensor, σ. It is P that is directly measured from the angular dependence of the paramagnetic frequency, ω_P.

That this form for H_P is appropriate is seen as follows. Let us assume that the polynuclear cluster can be represented by some total spin angular momentum and a g tensor in complete analogy with, say, a single transition-metal ion. The connection between the cluster angular momentum and g tensor with those quantities for exchange coupled constituent ions has been addressed by Griffith.[18] The dipolar Hamiltonian then has the usual form[19]

$$H_p = \sum_k \langle \mu \rangle^+ \cdot D_k \cdot I \tag{3}$$

where D_k is the dipolar coupling between the kth cluster and the nuclear spin, I. It is assumed that all clusters are equivalent, i.e., have the same magnetic moment, $\langle \mu \rangle$, in both magnitude and orientation. The dipolar coupling tensor in its principal axis system is

$$D_k^{PAS} = \frac{\gamma \hbar}{r_k^3} \begin{pmatrix} 1 & 0 & 0 \\ 0 & 1 & 0 \\ 0 & 0 & -2 \end{pmatrix} \tag{4}$$

As a practical convenience, the sum over clusters in eq 3 can be truncated to include only near neighbors for which $1/r_k^3$ is not negligible. Additionally, since for clusters the spin density can be spatially delocalized, then eq 3 can also be summed (or integrated) over sites of delocalization with an appropriate spin density weighting factor. The magnetic moment $\langle \mu \rangle$ has been calculated by Bloembergen[19] and for the high temperatures in this study is

$$\langle \mu \rangle = \beta^2 S(S+1) g^2 \cdot H_0 / 3 k_B T \tag{5a}$$

$$g^2 = R(g^{PAS})^2 R^+ \tag{5b}$$

In eq 5b, the orthogonal transformation, R, rotates g from its principal axis system into the lab frame ($z_{lab} || H_0$). The transformation U_k can be defined which rotates the dipolar tensor from its principal axis system into the g-tensor principal axis system, common to all clusters. Thus, the dipole coupling tensor, expressed in the lab frame, is

$$D_k = R[U_k D_k^{PAS} U_k^+] R^+ \tag{6}$$

Substituting eq 5 and 6 into eq 3 gives a Hamiltonian of the desired form (eq 2) where the coupling tensor P in the lab frame is

$$P = \frac{\beta^2 S(S+1)}{3 k_B T} R[(g^{PAS})^2 \sum_k U_k D_k^{PAS} U_k^+] R^+ \tag{7}$$

The relation between the tensors P and g is simple only in rather special cases. For example, if the relevant near-neighbor clusters all lie on a single axis which itself lies along one of the g-tensor principal axes, defined as g_{zz}^{PAS}, then the transformations U_k are all the identity operation and P, in its principal axis system, is just

$$P^{PAS} = \frac{\gamma h \beta^2 S(S+1)}{3 k_B T} \begin{pmatrix} (g_{xx}^{PAS})^2 & 0 & 0 \\ 0 & (g_{yy}^{PAS})^2 & 0 \\ 0 & 0 & -2(g_{zz}^{PAS})^2 \end{pmatrix} \sum_k r_k^{-3} \tag{8}$$

which is axially symmetric only if the g tensor is also axial. P becomes traceless and axial if g is isotropic. In the general situation, the principal axes of P will be oriented differently from those of either D_k or g.

If the anisotropy in g can be neglected, $g_{xx} = g_{yy} = g_{zz} = g$, then the following result is obtained for the observed paramagnetic shift, ω_P:

$$\omega_P = \frac{\omega_0 \beta^2 \mu^2}{3 k_B T} \sum_k (1 - 3 \cos^2 \theta_k) r_k^{-3} \tag{9}$$

where we have used the normal definition of the magnetic moment, $\mu^2 \equiv S(S+1)g^2$ in terms of an isotropic g factor. Here θ_k is the angle between the kth dipole vector and H_0 and ω_0 is the zero-order Zeeman frequency. The tensor P to which the angular-dependent shift corresponds depends on the explicit values of r_k and θ_k in the sum.

The magnetic susceptibility tensor, χ, for noninteracting spins[18]

$$\chi = \frac{N_a \beta^2 S(S+1)}{3 k_B T} g^2 \tag{10}$$

is then related to the principal components of P (measured in hertz) in the special case of eq 8 by

$$\chi_{ii} = \frac{N_a (2\pi P_{ii}/\gamma H_0)}{\sum_k r_k^{-3}} \qquad i = x, y$$

$$\chi_{zz} = \frac{-N_a (2\pi P_{zz}/\gamma H_0)}{2\sum_k r_k^{-3}} \tag{11}$$

and the value appropriate for powders is

$$\chi = \tfrac{1}{3}(\chi_{xx} + \chi_{yy} + \chi_{zz}) \tag{12}$$

Once the quadrupolar coupling and its angular dependence have been determined, then its evaluation in terms of molecular structure and ordering is well-understood as discussed elsewhere.[7] In short, we determine a symmetric traceless residual quadrupolar coupling tensor, $\langle V \rangle$. The two independent principal components (eigenvalues) of $\langle V \rangle$, $\langle V_{ii}^{PAS} \rangle$, can then be related to order parameters, S_{zz} and $S_{x^2-y^2}$, which are the first nontrivial moments of the orientational distribution function describing the spatial disorder of the probe. The disorder considered here is dynamic disorder with a reciprocal correlation time large compared to the static quadrupolar coupling of 175 kHz. Static disorder results in substantial broadening of resonance lines in single-crystal experiments but has no effect on powder patterns as compared to powder patterns of static ordered systems. The two-order parameters determined in this experiment are

$$S_{zz} = \langle P_2(\cos\theta) \rangle = \langle V_{zz}^{PAS} \rangle / \nu_Q \tag{12a}$$

$$S_{x^2-y^2} = (4\pi/5)^{1/2}(Y_{22}(\theta\phi) + Y_{2-2}(\theta\phi)) = (2/3)^{1/2}(\langle V_{xx}^{PAS} \rangle - \langle V_{yy}^{PAS} \rangle)/\nu_Q \tag{12b}$$

$$\nu_Q = 3/4e^2qQ/h \tag{12c}$$

The eigenvectors of $\langle V \rangle$ contain the direction cosines which describe the orientation of the frame in which S_{zz} and $S_{x^2-y^2}$ are determined relative to a reference frame such as the laboratory frame or some molecular frame.

Results and Discussion

Single-Crystal X-ray Structure of $[Fe_3O(O_2CCH_3)_6(4\text{-Me-py})_3](C_6H_6)$. This material crystallizes in the space group $R32$ with $Z = 3$. A drawing of the molecular structure is shown in Figure 2. The triply bridging oxygen atom resides at a site of 32 symmetry, with the iron atoms and the 4-methylpyridine ligands located on crystallographic 2-fold axes.

Table IV provides a comparison of selected bond distances in the title complex with those observed in three closely related Fe_3O complexes. In the title complex, the planes of the pyridine ligands are nearly parallel to that of the three iron atoms; the dihedral angle is 4.6°. This orientation differs from that observed[20] in the 3-Me-py analogue, where the ligands were nearly orthogonal to the Fe_3 plane, and from the 4-Et-py analogue[6,21] where two of the ligands are approximately perpendicular to the Fe_3 plane, while one is approximately parallel to this plane. The py complex[20] is isostructural with the title complex.

Notice that although a significant variation is observed in the Fe–O distances in cases where the complex is "valence-localized", for example, the 4-Et-py complex at 163 K, the average Fe–O

(18) Griffith, J. S. *Struct. Bonding (Berlin)* **1972**, *10*, 87.
(19) Bloembergen, N. *Physica* **1950**, *16*, 95.
(20) Strouse, C. E.; Inniss, D.; Oh, S. M.; Hendrickson, D. N., unpublished results.
(21) Oh, S. M.; Hendrickson, D. N.; Hassett, K. L.; Davis, R. E. *J. Am. Chem. Soc.* **1985**, *107*, 8009.

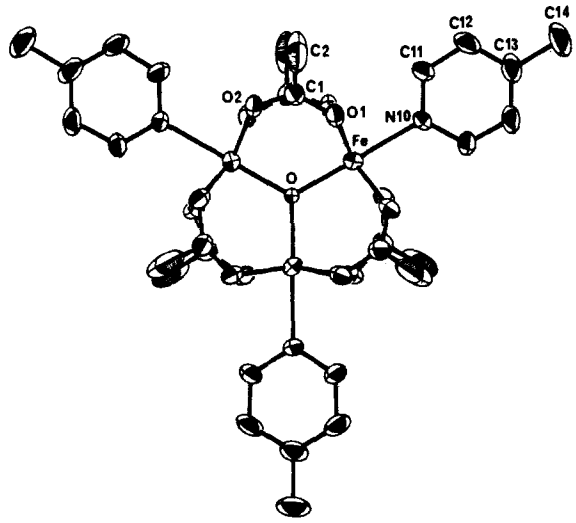

Figure 2. ORTEP of the molecular structure of $Fe_3O(O_2CCH_3)_6(4\text{-Me-py})_3$ in the benzene solvate compound **1**. Atoms are shown as 50% equiprobability ellipsoids.

Table IV. Bond Distances (Å) for $[Fe_3O(O_2CCH_3)_6(L)_3](S)$ Complexes. Values in Brackets Are Averages of Chemically Equivalent Distances

L	S	Fe–O	Fe–O_{ac}	Fe–N	ref
4-Me-py	C_6H_6	1.907 (1)	2.043 (3) 2.095 (3) ⟨2.069⟩	2.195	this work
py	py	1.909 (2)	2.066 (7) 2.078 (7) ⟨2.072⟩	2.224 (12)	20
4-Et-py	4-Et-py	2.011 (4) 1.856 (1) 1.856 (1) ⟨1.908⟩	⟨2.059⟩	⟨2.228⟩	6, 21
3-Me-py	3-Me-py	1.916 (2) 1.855 (2) 1.936 (2) ⟨1.902⟩	⟨2.056⟩	⟨2.227⟩	20

distances in all four complexes are essentially identical. Likewise, differences in the average Fe–O_{ac} distances are not significant. While the average Fe–N distances in the other three complexes are nearly identical, the Fe–N distance in the title complex is 0.03 Å shorter than the others. This is about 6 times the estimated standard deviation in the Fe–N distance. We offer no explanation for this anomaly.

The packing arrangement projected down the *c* axis is depicted in Figure 3. Along the *c* axis, complex molecules and solvate molecules occupy alternating sites of 32 symmetry (see Figure 4). The acetate groups of translationally equivalent complex molecules form a cavity in which the solvate molecule resides. Electron density maps reveal a preferred orientation of the benzene molecule with its local 6-fold axis perpendicular to both the crystallographic 3-fold and 2-fold axes. The large thermal parameters obtained for this group, however, are consistent with a dynamic disorder.

Another significant intermolecular interaction exists between the pyridine ligands in adjacent stacks. These stacks are related by the crystallographic 3_1 axis that passes through the pyridine ligand close to the midpoint between the two meta carbon atoms. The separation between these nearly parallel groups is $c/3 = 3.51$ Å. Since this is close to the optimum separation between aromatic groups, it would appear that the *c* lattice parameter and hence the size of the solvate cavity is controlled primarily by this interaction.

The high lattice symmetry of the present compound requires that in the absence of interaction with the benzene solvate or a cooperative interaction between molecular stacks, the three valence localized forms of the complex are degenerate. Since it is possible

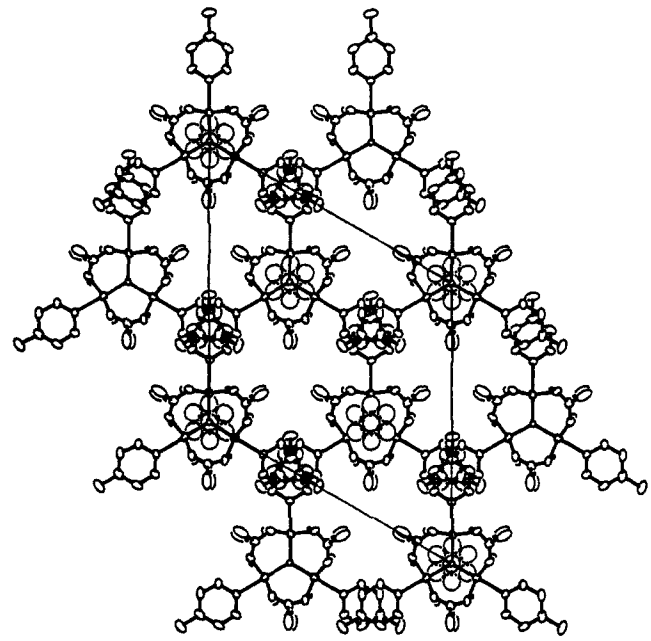

Figure 3. Packing arrangement in $[Fe_3O(O_2CCH_3)_6(4\text{-Me-py})_3](C_6H_6)$. The crystallographic *c* axis is toward the viewer.

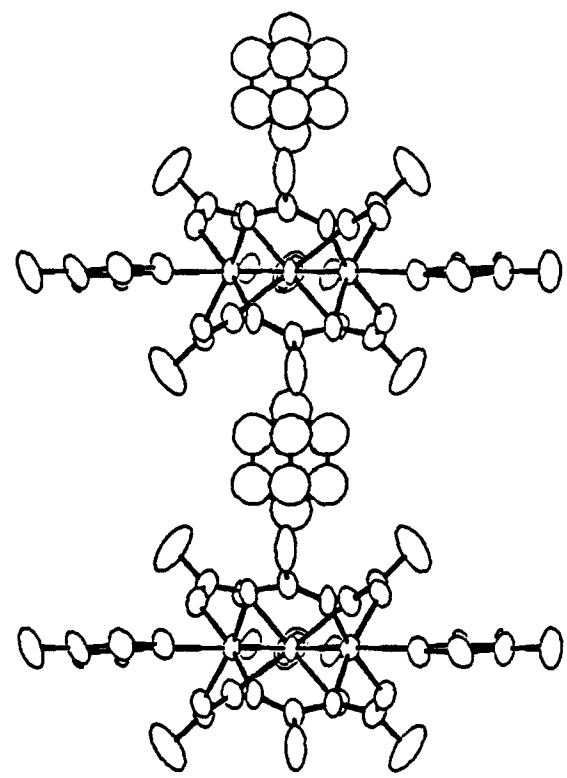

Figure 4. ORTEP view of the stacking along the *c* axis.

to alter this structure either by changing the solvate molecule or the ligand molecule, this high symmetry should make it possible to identify those factors that influence the intramolecular electron exchange rate.

^{57}Fe Mössbauer Spectroscopy. Variable-temperature Mössbauer spectra are illustrated in Figure 5 for **1**. At 8 K, the mixed-valence complex is localized on the Mössbauer time scale; that is, the rate of *intra*molecular electron transfer is less that $\sim 10^6$–10^7 s^{-1}. As can be seen in Figure 5, the 8 K spectrum can be least-squares-fit with two quadrupole-split doublets (Lorentzian line shapes). Parameters resultant from fitting to Lorentzian lines are collected in Table V. At 8 K, the fitting indicates that the Fe^{III} doublet is 64.2 (1)% of the spectral area, whereas the Fe^{II} doublet corresponds to 35.8 (1)%. This is quite close to the expected 2:1 ratio of Fe^{III}:Fe^{II}.

Table V. Mössbauer Fitting Parameters for $[Fe_3O(O_2CCH_3)_6(4\text{-Me-py})_3](C_6H_6)$[a]

	δ, mm/s[b]			ΔE_Q, mm/s			% area			Γ, mm/s[c]		
T, K	Fe^{III}	Fe^{av}	Fe^{II}	Fe^{III}	Fe^{av}	Fe^{II}	Fe^{III}	Fe^{av}	Fe^{II}	Fe^{III}	Fe^{av}	Fe^{II}
8	0.550 (1)		1.341 (1)	1.277 (1)		1.971 (2)	64.2 (1)		35.8 (1)	0.136 (1)		0.169 (2)
										0.133 (1)		0.175 (3)
61	0.554 (1)	0.773 (15)	1.329 (3)	1.222 (2)	0.359 (30)	1.885 (6)	52.2 (1)	20.4 (1)	27.4 (1)	0.160 (3)	0.334 (36)	0.194 (6)
										0.145 (2)	0.306 (23)	0.248 (10)
98	0.580 (1)	0.833 (16)	1.225 (5)	1.101 (2)	0.333 (32)	1.480 (10)	48.4 (2)	26.0 (1)	25.6 (1)	0.179 (3)	0.341 (39)	0.226 (11)
										0.141 (2)	0.305 (22)	0.346 (12)
104	0.583 (2)	0.747 (13)	1.047 (6)	0.930 (3)	0.319 (27)	1.235 (13)	48.8 (2)	27.8 (1)	23.6 (1)	0.147 (4)	0.245 (30)	0.190 (17)
										0.127 (3)	0.237 (26)	0.263 (15)
114	0.588 (2)	0.722 (36)	1.030 (11)	0.857 (4)	0.317 (73)	0.975 (19)	43.8 (2)	38.6 (2)	17.6 (1)	0.164 (5)	0.241 (35)	0.261 (41)
										0.124 (3)	0.271 (35)	0.257 (21)
200		0.677 (1)			0.416 (2)			100			0.146 (2)	
											0.131 (1)	
298		0.653 (1)			0.520 (2)			100			0.130 (2)	
											0.127 (2)	

[a] Peaks were least-squares-fit to Lorentzian line shapes with equal areas for both components of a doublet; error in the last significant figure is given in parentheses. [b] Center shifts relative to Fe metal. [c] Half-width at half-maximum listed in order of increasing velocity of the peak.

Table VI. Fitting Parameters for the Simulated Spectra from the Relaxation Model

	δ, mm/s[a]		ΔE_Q, mm/s[b]				
T, K	Fe^{III}	Fe^{II}	Fe^{III}	Fe^{II}	rate, $1/\tau$	$P(Fe^{II})$[c]	K^+/K^-[d]
8	0.55	1.34	1.28	1.97	2.4×10^2	0.324	1.04
61	0.55	1.31	1.22	1.89	1.6×10^6	0.323	1.14
98	0.54	1.29	1.20	1.62	2.1×10^7	0.328	1.34
104	0.56	1.24	1.19	1.51	3.4×10^7	0.328	1.30
114	0.53	1.30	1.24	1.38	5.1×10^7	0.332	1.46
123	0.51	1.27	1.18	1.29	8.3×10^7	0.348	0.97
130	0.49	1.21	1.20	1.21	1.1×10^8	0.331	1.14
135	0.46	1.20	1.24	1.23	2.5×10^8	0.342	1.01
200	0.45	1.14	1.20	1.15	2.0×10^9	0.321	0.99
298	0.43	1.11	1.24	0.92	2.2×10^9	0.314	0.93

[a] The center shift is relative to Fe metal. [b] The signs of the electric field gradients at the Fe^{III} and Fe^{II} sites are opposite to each other. [c] The fraction of the Fe^{II} site is represented. [d] The ratio of the intensities between the positive (negative) velocity component and the negative (positive) velocity component of the Fe^{III} (Fe^{II}) sites.

An increase in the temperature of **1** leads to an increase in the rate of intramolecular electron transfer such that above ~200 K, the rate exceeds the $\sim 10^7$–10^8-s^{-1} value that can be sensed by the Mössbauer technique. At 298 K, a single *average* quadrupole-split doublet is seen. The isomer shift of 0.653 (1) mm/s vs. iron foil observed for this 298 K doublet is only consistent with it being attributable to an average doublet resulting from rapid electron transfer.

The spectra obtained from ~60 to 200 K present an appreciable challenge to interpret and fit (simulate). Two different analytical approaches were tried. Following the lead of Brown et al.,[22] the three-site relaxation model developed with the approach of Wickman[23] can be used to try to simulate the appearance of the spectra at various temperatures. If $1/\tau_A$ is the probability of state A (Fe^{II}) changing and $1/\tau_B$ is that of state B (Fe^{III}), a steady state is reached when $P_A/\tau_A = P_B/\tau_B$, where P_A and P_B are the fractional populations of states A and B, respectively. The overall relaxation time is given as $\tau = \tau_A\tau_B/(\tau_A + \tau_B)$. In addition to the two relaxation time parameters, it is necessary to specify isomer shifts, quadrupole-splitting values, signs of electric-field gradients, and spectral line widths for the Fe^{II}- and Fe^{III}-type sites at each temperature. The literature[22,23] should be consulted for details. In Figure 6 are given the best simulations that could be obtained for the experimental spectra in Figure 5. In Figure 6, the value for the relaxation rate (i.e., $1/\tau$) is given for each simulated spectrum. In Table VI are given the parameters that were used to generate the simulated spectra of Figure 6. Two comments are in order. First, in order to generate the spectra shown in Figure 6, it was necessary to assume that the *signs* of the electric field gradients at the Fe^{II} and Fe^{III} sites are opposite to each other. This does not seem unreasonable. Second, in order to mimic the line shapes seen in the experimental spectra, it was necessary to artificially increase the relative intensity (area) associated with the positive (and negative) velocity component of the Fe^{III} (and Fe^{II}) sites. The necessity for this can be readily seen in a comparison of the 8 and 61 K spectra. Compared to the situation in the 8 K spectrum, these peaks in the 61 K spectrum seemingly have grown in intensity.

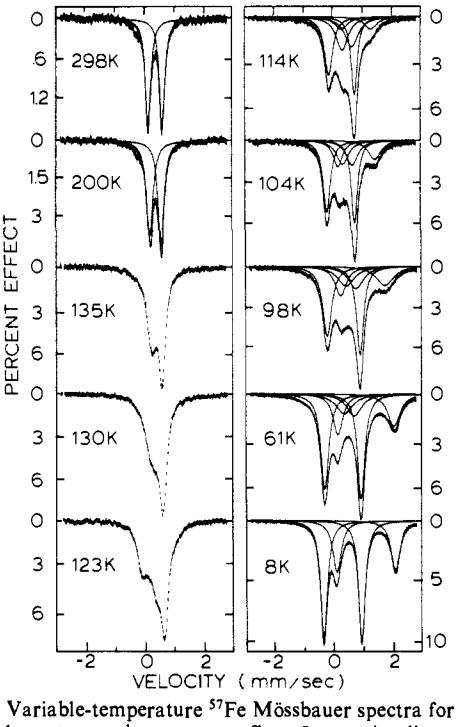

Figure 5. Variable-temperature ^{57}Fe Mössbauer spectra for compound **1**. Several spectra are least-squares fit to Lorentzian lines.

(22) Dziobkowski, C. T.; Wrobleski, J. T.; Brown, D. B. *Inorg. Chem.* **1981**, *20*, 679.
(23) Wickman, H. H. In *Mössbauer Effect Methodology*; Gruverman, I. J., Ed.; Plenum: New York, 1966; Vol. 2.

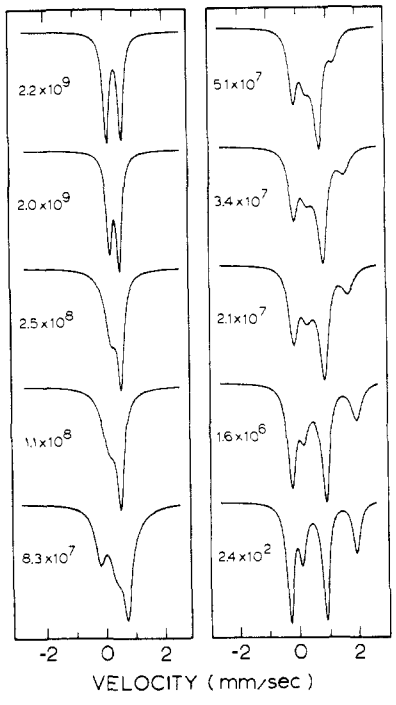

Figure 6. Simulations of the Mössbauer spectra of compound 1 (see Figure 5) obtained from a three-site relaxation model.

The results obtained from the second analytical approach give some insight into why it was necessary to artificially increase the intensity of certain features in the three-site relaxation simulation. As can be seen in Figure 5, it is possible to least-squares-fit the Mössbauer spectra obtained in the ~61–114 K region with *three* quadrupole-split doublets (fitting parameters are given in Table V). The spectra at higher temperatures do not show features that are well-resolved enough for this approach. In each case, there is a Fe^{II} and a Fe^{III} doublet in the approximate ratio of 1:2. The characteristics of the third doublet indicate that it corresponds to Fe_3O complexes that are delocalized on the Mössbauer time scale. The area of this third doublet varies from 20.4% at 61 K to 38.6% at 114 K. A "third doublet" is *not* visible in a spectrum run at 36 K.

The relatively sudden appearance of delocalized species in the ~60-70 K region is likely associated with an order–disorder phase transition. Two phase transitions (~112 and ~190 K) are visible in the heat capacity data[10,24] obtained for $[Fe_3O(O_2CCH_3)_6(py)_3](py)$, **3**, where py is pyridine. This compound is isostructural with **1**. The ~112 K phase transition seen for **3** has been assigned to an order–disorder phase transition, wherein at temperatures below 112 K the distorted Fe_3O complexes (i.e., electronically localized with one Fe^{II} and two Fe^{III} ions) have their senses of distortion ordered throughout domains in the crystal. The overlap of pyridine ligands between Fe_3O complexes in different stacks provides the driving force for this ordering. At ~112 K, thermal energy exceeds this *inter*molecular interaction energy and the senses of distortion of Fe_3O complexes become disordered throughout the crystallite. It is likely that when this occurs, the potential energy diagram of each Fe_3O complex changes such that the energy of the undistorted complex becomes comparable to that of the distorted complex.[25-28] Thus, there are four approximately equal-energy minima in the potential energy surface (three minima for the three possible distortions and one minimum for the undistorted complex case). If this analysis is correct, it is clear why the three-site relaxation model did not work well. A four-site relaxation model is needed.

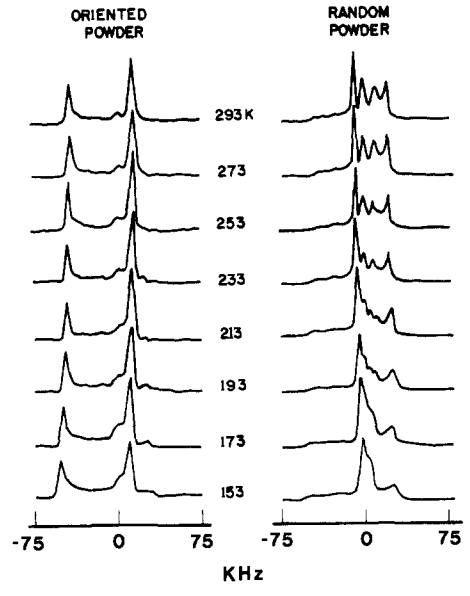

Figure 7. ^2H NMR spectra of magnetically oriented and random powder samples as a function of temperature. Spectra were from 512 transients using a two-pulse solid echo with a pulse spacing of 35 μs.

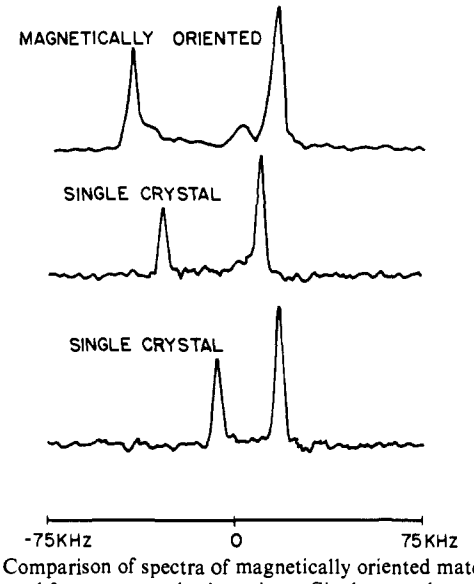

Figure 8. Comparison of spectra of magnetically oriented material and a single crystal for two general orientations. Single-crystal spectra were acquired with 1024 transients and a 1-s recycle delay using the four-pulse echo sequence described in the Experimental Section.

^2H NMR Spectroscopy. Shown in Figure 7 as a function of temperature are ^2H NMR spectra of magnetically oriented and random powder samples of **1**. The magnetically oriented spectra were obtained by the simple expedient of very loosely packing the microcrystalline material in the sample tube. In the 5.9-T field, the microcrystals torque and align along their easy axes of magnetization. The random powder spectra were obtained by tightly packing (outside the magnetic field) the samples in tubes with a pistonlike lid. The spectrum from the magnetically oriented material is compared with spectra obtained from a single crystal in two general orientations in Figure 8. The single-crystal spectra quite generally show a smaller line width, 2 kHz rather than 5 kHz, indicating that in the magnetically ordered samples, ordering along H_0 is not perfect. Several important qualitative features are immediately apparent. First, all the spectra, i.e., those obtained from single crystals, magnetically or randomly oriented powders, are not symmetric about the isotropic ^2H NMR frequency. This indicates that both paramagnetic interactions with the trinuclear

(24) Sorai, M.; Kaji, K.; Hendrickson, D. N.; Oh, S. M. *J. Am. Chem. Soc.* **1986**, *108*, 702.
(25) Kambara, T.; Hendrickson, D. N.; Sorai, M.; Oh, S. M., submitted for publication in *J. Chem. Phys.*
(26) Borshch, S. A.; Kotov, I. N.; Bersuker, I. B. *Chem. Phys. Lett.* **1982**, *89*, 381.
(27) Launay, J. P.; Babonneau, F. *Chem. Phys.* **1982**, *67*, 295.
(28) Cannon, R. D.; Montri, L.; Brown, D. B.; Marshall, K. M.; Elliott, C. M. *J. Am. Chem. Soc.* **1984**, *106*, 2591.

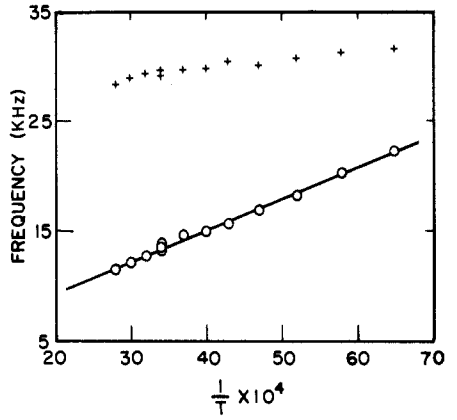

Figure 9. Plots of ω_Q (+) and ω_P (O) vs. $1/T$ obtained from the spectra of magnetically oriented $[Fe_3O(O_2CCH_3)_6(4\text{-Me-py})_3](C_6D_6)$.

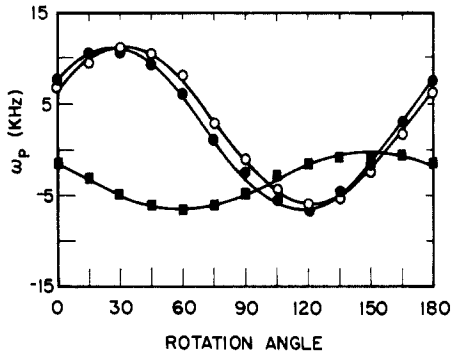

Figure 10. Rotation patterns for ω_P as a function of the goniometer angle about three orthogonal axes at 293 K.

iron clusters (i.e., through-space dipolar interactions) and quadrupolar coupling determine the resonance frequencies. Second, the breadths of the random powder patterns (~−58 to ~32 kHz) over the entire temperature range from 293 to 153 K are small compared to that expected for rigid aromatic deuterons (−140 to +140 kHz). Thus, the solvate benzene molecule in **1** undergoes a substantial degree of rapid ($\tau_c < 5 \times 10^{-5}$ s) motional averaging. Since the powder pattern breadth does not change substantially over the temperature range examined, it is concluded that the nature of the dynamical averaging also varies little with temperature. Third, for both the magnetically oriented and the general orientation of the single-crystal spectra, a single quadrupolar doublet is always observed. This requires that the rapid dynamical process must have axial symmetry about the local C_6 axis of the benzene solvate molecule in order that the six deuterons are magnetically equivalent.

From the resonance frequencies of the doublet, as observed in the spectra of magnetically oriented material, the residual quadrupolar coupling frequency, ω_Q, and the paramagnetic shift, ω_P, are determined as in Figure 1 and plotted vs. $1/T$ in Figure 9. The paramagnetic frequency, dependent on the local magnetic field from neighboring clusters, increases at lower temperatures and shows a linear Curie law behavior, whereas the quadrupolar coupling, reflective of the dynamical averaging process, decreases only slightly at higher temperatures. Over the temperature range investigated, a single Curie constant of 2.88×10^3 kHz K is found. At lower temperatures, deviations might be expected as the cluster spin state populations change.

Plots of ω_Q and ω_P for the three-axis single-crystal rotation study at 293 K are shown in Figure 10. The angular dependence of ω_p is in accord with the Hamiltonian of eq 3. The principal components of the tensors $\langle V \rangle$ and P and the Euler angles determined from these data are listed in Table VII.[29] The Euler

(29) (a) Barnes, R. G. *Adv. Quadrupole Reson.* **1974**, *4*, 335. (b) The Euler angle α is not listed since the anisotropy $(T_{xx} - T_{yy})$ in these tensors is comparable to the experimental error and is thus poorly determined.

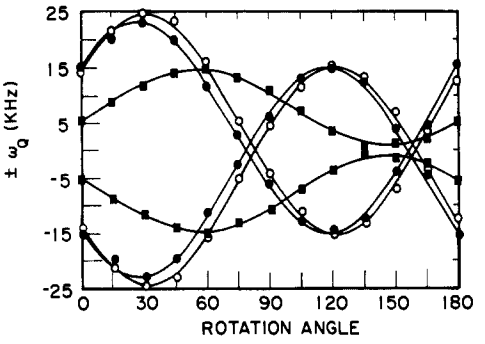

Figure 11. Rotation patterns for ω_Q as a function of the goniometer angle about three orthogonal axes at 293 K.

Table VII. Principal Components and Orientation of the Paramagnetic and Residual Quadrupolar Tensors, P and $\langle V \rangle$, Respectively, for the Deuteriobenzene Solvate Molecule. Euler Angles Are Relative to the Principal Axes of P with the Convention That the System Is Right-Handed and the Large Component of P Is along the z Axis

	principal components T, kHz			Euler angles, deg	
tensor	T_{xx}	T_{yy}	T_{zz}	β	γ
P	−6 ± 1.5	−8 ± 1.5	14 ± 1.5	0	0
$\langle V \rangle$	−14 ± 1.5	−18 ± 1.5	32 ± 1.5	±2	±4

angles for $\langle V \rangle$ are referenced to the principal axis frame of P. This choice of reference frame arises naturally since we find that the largest component of P, −14.7 kHz, is just the value of ω_P that is observed from the magnetically oriented sample at the same temperature. Thus, the large components of the P and the magnetic susceptibility tensors are parallel. From the crystal morphology of the NMR sample, it was estimated that the crystallographic C_3 axis which is perpendicular to and passes through the center of the triangular cluster plane and the solvate molecule is along the largest component of the experimentally determined paramagnetic tensor P. In addition, NMR experiments on the closely related compound, $[Fe_3O(O_2CCD_3)_6(py)_3](py)$, which crystallizes in the same space group $R32$, show that a single crystal magnetically orients exactly along the crystallographic C_3 axis. This is a convenient reference frame for discussing these experiments since its z axis is parallel to the molecular C_3 axis and the largest components of both the magnetic susceptibility and P.

From Table VII, it is seen that the residual quadrupolar coupling tensor $\langle V \rangle$ is approximately axially symmetric with the large component also along the molecular C_3 axis. The two relevant order parameters in this frame, calculated according to eq 12a and 12b and by using the data of Table VII (293 K), are $S_{zz} = 0.24$ and $S_{x^2-y^2} = 0.02$. Any model proposed to describe the benzene solvate molecule dynamics must be consistent with both the order parameters and the orientation in the molecular frame.

Since the tensors $\langle V \rangle$ and P have a fixed relative orientation in the molecular frame, powder patterns must reflect this. For example, from Table VII, the large principal components of $\langle V \rangle$ and P are 32 and 15 kHz, respectively, and are, within experimental error, parallel. Consequently, the powder pattern at the corresponding temperature of 293 K should extend to just 47 kHz, which indeed it does. The use of powder pattern simulations for this purpose is probably substantially less precise than single-crystal experiments since in the general case the simulation depends on all three Euler angles as well as accurate experimental line shapes, somewhat difficult to obtain in these NMR echo experiments since the paramagnetic and quadrupolar shifts are comparable and must be refocused simultaneously in order to get accurate powder patterns.

The order parameters and direction cosines determined from the single crystal at 293 K show that the magnitude of the residual quadrupolar coupling is reduced by a factor of 4 ($S_{zz} = 0.24$) and there is approximate axial symmetry about the molecular C_3 axis

($S_{x^2-y^2}$ = 0.02). From ongoing X-ray studies[20] of the related molecule, $[Fe_3O(O_2CCH_3)_6(py)_3](py)$, from 300 to 200 K there is a C_3 axis present. At ~200 K the C_3 axis is lost. This could be the result of the pyridine solvate molecules rotating rapidly above ~200 K, but below this temperature these solvate molecules stop rotating about the C_3 axis. Dynamics involving the rotation of the benzene solvate molecules of **1** about the C_3 axis of the stacks combined with reorientation of each benzene molecule about its local C_6 axis would explain the order parameters observed for **1**. Either one of these two motions of the benzene solvate molecules about an axis reduces S_{zz} by a factor of $P_2(\cos\theta)$, where θ is the angle subtended by the C–D bond and the axis of reorientation, and brings the large component of $\langle V \rangle$ along the motional axis. Thus, the orientation about the local C_6 axis makes the six benzene deuterons equivalent and results in an "intermediate" order parameter of magnitude of 0.5 (i.e., θ is 90°), with the large component perpendicular to the C_3 axis. Since the experimental value of S_{zz} is 0.24, clearly additional dynamical averaging exists. This additional process is then properly visualized by considering the reorientation of the vector normal to the benzene plane. Since the final average orientation is symmetric about the molecular C_3 axis, then the motion of this vector is also symmetric about this axis. If the vector is restricted to move in the plane perpendicular to the C_3 direction either continuously or by 3-fold jump motions, then an additional 2-fold reduction in the order parameter to S_{zz} = 0.25 occurs, as is experimentally observed. Thus, our picture of benzene solvate dynamics for this molecule is simply reorientation about the local C_6 axis and reorientation of this local axis about the molecular C_3 axis. The results from random and magnetically ordered powders indicate little change of this picture over the temperature range from 153 to 293 K. In agreement with this, we note that preliminary thermal analysis measurements[30] show no thermal effects over this temperature range.

The primary source of temperature dependence in the ^2H NMR spectra arises from the Curie law behavior of the paramagnetic shifts. The dipolar shifts for a given benzene solvate molecule will result primarily from the Fe_3O complexes directly above and below it. From the above considerations regarding the solvate dynamics, the average point in space for the solvate deuterons is just the center of the benzene molecule, and thus, each deuteron is on average about 5.3 Å from the center of each of the two nearest Fe_3O complexes. Next, nearest Fe_3O complexes are at a distance of 12 Å and as a reasonable approximation can be neglected. Consequently, the dipolar coupling tensors both lie along the C_3 axis which is along the large component of the magnetic susceptibility and satisfy the special geometry assumed in eq 8. With the usual definition of $\mu_{ii}^2 = S(S+1)g_{ii}^2$ and the data from Table VII, we calculate $|\mu_{xx}| = (4.0 \pm 0.5)\mu_B$, $|\mu_{yy}| = (4.7 \pm 0.5)\mu_B$, and $|\mu_{zz}| = (4.4 \pm 0.5)\mu_B$, or an average cluster magnetic moment of $(4.3 \pm 0.5)\mu_B$. Clearly the anisotropy in the cluster g tensor is small. The magnetic moment of $|\mu| = (4.3 \pm 0.5)\mu_B$ is, however, somewhat smaller than the value of $5.9\mu_B$ determined from powder magnetic susceptibility measurements.[31] Thus, the observed paramagnetic shifts are somewhat smaller than expected based on our analysis, c.f., eq 8 or 9. Inclusion of the next two nearest neighbors at r_k = 12 Å and $\theta_k \approx 90°$ in the calculation makes a small but negligible improvement. If we assume that the value of $\mu = 5.9\mu_B$ from the powder susceptibility experiments is appropriate to this calculation, then from eq 9 we conclude that the assumed values of $\theta_k = 0°$ and/or r_k = 5.3 Å are too small. Qualitatively this result is in accord with the electron spin not localized at the center of the cluster but rather delocalized. To account qualitatively for this, we assume now that the spin density is delocalized at the three iron sites 2 Å from the center of the cluster. This will still result in an overall P tensor with its large component along the C_3 axis, but it arises from three dipolar couplings with each of the two clusters, with r_k = 5.7 Å and θ_k = 21° when the C_3 axis is parallel to H_0. From eq 9, this gives $\omega_P = -15$ kHz which compares very well with the appropriate principal component $P_{zz} = -14.7$ kHz.

(30) Oh, S. M.; Hendrickson, D. N., unpublished results.
(31) Hendrickson, D. N.; Oh, S. M.; Dong, T.-Y.; Kambara, T.; Cohn, M. J.; Moore, M. F. *Comments Inorg. Chem.* **1985**, *4*, 329.

Conclusion and Comments

The 133 K X-ray structure of $[Fe_3O(O_2CCH_3)_6(4\text{-Me-py})_3](C_6H_6)$ shows that the Fe_3O complex molecules are stacked along a 3-fold crystallographic axis. The benzene solvate molecules are intercalated into the stacks such that the plane of the benzene solvate is perpendicular to the Fe_3O planes; the solvate molecules are disordered about the C_3 axis. The variable-temperature Mössbauer results indicate that the *intra*molecular electron transfer in each mixed-valence complex is fast from 298 to ~135 K, but below this temperature the rate of electron transfer decreases with decreasing temperature until a temperature of ~36 K, below which localized Fe^{II} and Fe^{III} sites are present. Detailed ^2H NMR studies, including variable-temperture work on magnetically oriented samples and a single-crystal study, clearly established that the benzene solvate molecule throughout the range of 293–153 K is both rotating rapidly about a local C_6 axis and rotating rapidly about the C_3 axis that runs down each stack of Fe_3O complexes.

Due to the near electronic degeneracy in these mixed-valence Fe_3O complexes, they serve as very sensitive probes of the nature of the solid state. It is our hypothesis[6,10] that the temperature dependence that is seen in the Mössbauer spectra for several of these mixed-valence Fe_3O complexes is *not* just the result of directly thermally activating these complexes to overcome a potential energy barrier for electron transfer. The solid-state environment plays a crucial role. Dynamics of solvate molecules and/or ligands dramatically affect the rate of intramolecular electron transfer in a given Fe_3O complex. The onset of dynamical motion in the solid at a certain temperature modifies the environment about a complex. The new environment changes the potential energy barrier such that intramolecular electron transfer can occur at a considerably faster rate. An overview of research in this area is available.[31]

In the case of $[Fe_3O(O_2CCH_3)_6(4\text{-Me-py})_3](C_6H_6)$, we would suggest that the onset of rotation of the benzene solvate molecules about the C_3 axes down the stacks of Fe_3O complexes leads first to a change in the potential energy diagram for each mixed-valence complex. The barrier(s) for intramolecular electron transfer will be reduced because the environment of benzene molecules rapidly rotating now has the C_3 symmetry required for rapid electron transfer between the three iron ions in a given Fe_3O complex. As a final comment, it should be noted that this transformation in the solid state from static to dynamic benzene solvates likely involves a phase transition. Interactions that occur between benzene solvate molecules and neighboring Fe_3O complexes within one stack or between ligand molecules in adjacent stacks could lead to the cooperativity that is the essence of a phase transition. In a very recent theoretical paper,[25] we summarized the various types of order–disorder and electronic localization–delocalization phase transitions that could occur in these mixed-valence Fe_3O complexes. Variable-temperature heat capacity measurements now in progress[32] on $[Fe_3O(O_2CCH_3)_6(4\text{-Me-py})_3](C_6H_6)$ should add to our understanding of the structural and electronic changes this material undergoes.

Acknowledgment. We are grateful for support from National Institutes of Health Grant HL13652 (D.N.H.) and from National Science Foundation Grants PCM-8118912 (R.J.W.) and CHE-8340836 (C.E.S.).

Registry No. $[Fe_3O(O_2CCH_3)_6(4\text{-Me-py})_3](C_6H_6)$, 101420-29-5; $[Fe_3O(O_2CCH_3)_6(H_2O)_3]$, 36354-69-5; D_2, 7782-39-0.

Supplementary Material Available: Tables of magnetic susceptibility data and observed and calculated structure factor amplitudes and anisotropic thermal parameters for the 133 K X-ray structure determination of $[Fe_3O(O_2CCH_3)_6(4\text{-Me-py})_3](C_6H_6)$ (8 pages). Ordering information is given on any current masthead page.

(32) Sorai, M.; Oh, S. M.; Hendrickson, D. N., unpublished results.